6

On Modeling Oil Borehole Logs Using Local Fractal Processes: A Case Study from Algeria

6 On Modeling Oil Borehole Logs Using Local Fractal Processes: A Case Study from Algeria

Said Gaci

Sonatrach, Division Exploration, Boumerdès, Algeria. Email: said_gaci@yahoo.com

Summary

This chapter deals with the characterization of subsurface heterogeneities by studying the spatial regularity variation of well logs. The local regularity of these signals, considered as multifractional Brownian motions (mBms) paths, is measured by the local Hölder exponent H related to the fractal parameter (or the Hurst exponent).

A regularity analysis is performed on datasets measured at four Algerian oil wells drilled in different geological contexts. It allows to extract information pertaining to subsurface.

It is shown that the derived regularity profiles, or the Hölder exponent functions, mainly those derived from sonic, density and neutron logs, show a clear correlation with lithology, and the lithological discontinuities correspond to sudden variations of H value. Moreover, for a given well, the obtained regularity logs exhibit a strong correlation between them. Therefore, the regularity is a robust property which can be successfully used to characterize lithological heterogeneities of layers. However, this study does not draw any relation between the recorded physical property and its estimated regularity degree for each log.

6.1 Introduction

Well logging consists of making a detailed record of rock and fluid properties to find hydrocarbon zones in the geological formations intersected by a borehole. During this operation, the logging tool is lowered on the end of a wireline into the open wellbore to measure the rock and fluid properties of the formation. Measurements include electrical properties (resistivity and conductivity at various frequencies), acoustic properties, radioactive, electromagnetic, nuclear magnetic resonance, and other properties of the rocks and their contained fluids. An interpretation of these measurements is then carried out in order to locate and quantify potential depth zones containing hydrocarbons.

Fractal geometry offers an appropriate framework for investigating the spatial heterogeneities of different geological patterns (Mandelbrot, 1975, 1977). Thanks to its success, this geometry has gained a widespread acceptance in various fields of geosciences, particularly in oil and gas engineering. Statistical fractals were introduced for the first time by Hewett (1986) to model well logs. Then, Hardy and Beier (1994) demonstrated that the well log behavior can be fitted with the fractional Brownian motion (fBm).

The fBm is a non-stationary stochastic fractal model with stationary increments. It is indexed by a Hurst exponent ($0<H<1$) quantifying its self-similarity degree. This process exhibits a local regularity H everywhere, thus, it is not suitable for studying signals whose regularity varies in time/space, which is the case for most geophysical signals. As a consequence, a generalization of the fBm, known as a multifractional Brownian motion (mBm), is obtained by allowing H to evolve in time (and/or space).

Though no longer stationary nor self-similar, compared to fBm, the mBm process is very versatile and useful to model real signals characterized by a

punctual time (or space) changing regularity. It received increasing attention in various research disciplines: geophysics (Wei et al. 2004; Wanliss, 2005; Wanliss and Cersosimo, 2006; Cersosimo and Wanliss, 2007; Echelard et al., 2010 ; Keylock, 2010; Gaci et al., 2010, 2011; Gaci and Zaourar, 2010, 2011a, 2011b; Luo et al., 2012), image processing (Bicego and Trudda, 2010), traffic phenomena (Li et al., 2007), etc.

In previous works (Gaci et al., 2010; Gaci and Zaourar, 2010, 2011a), sonic well logs were assumed to be mBm processes. Then, the depth-dependent regularity profiles derived from the logs allowed to perform a lithological segmentation, and to investigate heterogeneities of the geological layers crossed by the well. In this paper, the regularity analysis is extended to sets of well logs recorded in four Algerian oil boreholes. The data collection contains P- and S-wave sonic, bulk density, neutron porosity, Gamma ray, electrical resistivity, photoelectric absorption factor and natural gamma ray spectroscopy logs. In addition to the lithological regularity-based segmentation, this study attempts to check for the existence of a possible relation between the physical measurement values and their computed local Hölder exponents, and quantify the correlations between them for each analyzed well log.

This paper is structured as follows: Firstly, we give a short mathematical description of the fractal models (fBm and mBm), and the method of estimating their associated local Hölderian regularity. Secondly, an overview on the used well log measurements is presented, followed by a lithological description of the logged interval in the borehole. Thirdly, the results obtained from the well logs are presented and discussed. Finally, we conclude by recapitulating the main findings and giving the perspectives of our research.

6.2 Theory

6.2.1 Local Regularity

The Hölder exponent is the most generally mathematical tool used to quantify the regularity of a signal at any given point. For a stochastic process X whose trajectories are continuous but nowhere differentiable, it is defined by:

$$\alpha_X(z_0) = \sup\left\{\alpha,\ \limsup_{h\to 0} \frac{|X(z_0+h)-X(z_0)|}{|h|^{\alpha}} = 0\right\} \quad (1)$$

From the geometrical point of view, this definition means that the increments $X(z)-X(z_0)$ in the neighborhood of z_0 are included in a Hölderian envelope defined by $|X(z)-X(z_0)|^{\alpha_X(z_0)}$. The larger $\alpha_X(z_0)$, the smoother the signal at z_0 and vice-versa.

6.2.2 Fractional Brownian Motion

The fractional Brownian motion (fBm) is one of the most popular stochastic fractal models. It was introduced by Kolmogorov (1940) and developed by Mandelbrot and Van Ness (1968).

The fBm $B_H = \{B_H(z), z>0\}$ is a zero-mean Gaussian process with autocorrelation function:

$$E[B_H(z).B_H(s)] = \frac{\sigma^2}{2}\left[|z|^{2H} + |s|^{2H} + |z-s|^{2H}\right] \quad (2)$$

where $0<H<1$ is called the Hurst parameter, $\sigma>0$, $s>0$ and E[.] denotes the expected value (for H=1/2, the obtained process is the Brownian motion B(t)).

This process exhibits a short-range dependence for 0<H<1/2, independence for H =1/2 (Brownian motion), and long-range dependence for 1/2<H<1.

From the regularity point of view, it is proved that its pointwise Hölder exponent is almost surely equal to H at every point z. The higher the H value, the smoother the fBm trajectories.

6.2.3 Multifractional Brownian Motion

Due to its constant regularity, the fBm is not suitable for the analysis of signals exhibiting a time/space-varying regularity. To get rid of this drawback, multifractional Brownian motion (mBm) was introduced by allowing H to vary over depth (Peltier et Lévy-Véhel, 1995; Benassi et al., 1997a).

The mBm with the functional parameter H(z) is the zero-mean Gaussian process defined as:

$$W_{H(z)}(z) \propto \int_{-\infty}^{0} \left[(z-s)^{H(z)-1/2} - (-s)^{H(z)-1/2} \right] dB(s) + \int_{0}^{z} \left[(z-s)^{H(z)-1/2} \right] dB(s) \qquad (3)$$

where $H:[0,\infty) \to (0,1)$ is a Hölder continuous function. If $H(z)$ is constant, $W_{H(z)}(z)$ is reduced to a simple fBm.

The mBm possesses increments, which are generally neither independent nor stationary. Unlike fBm, pointwise Hölder exponent $\alpha_{W_H}(z)$ may depend on the location and can be described via the functional parameter H(z): at each z, $\alpha_{W_H}(z)$ is equal to $H(z)$ with probability one (Peltier and Lévy -Véhel 1995; Benassi et al., 1997b; Ayache and Taqqu, 2005). This property is very useful to model phenomena whose punctual regularity is time (and/or space) changing,

and makes mBm extremely versatile.

6.2.4 Pointwise Estimation of the Hölderian Regularity of mBm

Due to its accuracy and simplicity, the algorithm suggested by Peltier and Lévy-Véhel (1994) is used for estimating the local regularity of mBm paths. It is based on the local growth of the increment process $S_{k,n}(i)$ defined as:

$$S_{k,n}(i) = \frac{m}{n-1} \sum_{j \in [i-k/2, i+k/2]} |X(j+1) - X(j)|, \ 1<k<n \tag{4}$$

where n is the signal length, k is a fixed window size, and m is the largest integer not exceeding n/k.

The local Hölder function H(z) at the point $z = i/(n-1)$ is given by

$$\hat{H}(i) = -\frac{\log\left[\sqrt{\pi/2}\ S_{k,n}(i)\right]}{\log\ (n-1)} \tag{5}$$

6.3 Well Log Measurements

A well log is a continuous record versus depth or time, or both, of one or more physical quantities in or around a well. It is taken downhole, transmitted through a wireline to surface and recorded there. In oil and gas exploration, many physical formation properties are measured and interpreted in order to locate reservoir intervals. The logs used in our study are P- and S-wave velocities (Vp and Vs), bulk density (rhob), neutron porosity (nphi), Gamma ray (GR), electrical resistivity (LLD, AT20 and AT90), photoelectric absorption factor (PEF) and natural gamma ray spectroscopy (Th, U and K).

In the following, a short description of the well logs investigated in this study

is presented. More details can be found in the Oilfield Glossary, available at: http://www.glossary.oilfield.slb.com.

A sonic log displays traveltime of acoustic waves versus depth. This transit time measures the capacity of a geological formation to transmit seismic waves. Indeed, this capacity varies with lithology and rock textures, and decreases with an increasing effective porosity. The sonic log can then be used to calculate the porosity of a formation, a very useful property for hydrocarbon exploration.

A density log is a continuous record of a formation's bulk density along the length of a borehole. Identically to sonic and neutron logs, it is commonly used to calculate porosity. The density measurement is based on the reduction in gamma ray flux between a source and a detector due to Compton scattering. It consists of emitting gamma rays and recording the gamma rays radiating from the formation. The recorded gamma rays are connected to the electron density of the atoms in the material between source and detector, and thus to the average bulk density of the formation.

A neutron porosity log is recorded by bombarding the formation with neutrons. Hydrogen shows the biggest effect capturing neutrons. Since hydrogen is found mainly in the pore fluids, the neutron log responds principally to the formation porosity.

Gamma ray (GR) logs, usually recorded in API units, measure the natural radioactivity of a formation. Different types of rocks emit different amounts of natural gamma radiations. Since shales contain radioactive elements, they emit more gamma rays than other sedimentary rocks. Sandstones/carbonate, on the other hand, emit very few gamma rays. This difference in radioactivity between rocks allows the gamma tool to distinguish between shales and non-shales.

Resistivity logs, expressed in ohm-m, record the resistivity of the penetrated formation. They can take a wide range of values, and, therefore, for convenience are usually presented on a logarithmic scale. The resistivity property is used to determine the types of fluids present in the reservoir rocks. Hydrocarbons do not conduct electricity (high resistivities) while all formation waters do (low resistivities). In practice, several resistivity tool designs can be found, but the main difference between them lies in their investigation depth and their vertical resolution.

The photoelectric log measures the unitless photoelectric absorption factor, PEF, which is proportional to the average atomic number of the formation. Since fluids have very low atomic numbers, their corresponding PEF is very low. Dolomites, limestones, clays, heavy minerals and iron-bearing minerals present high PEF while sandstones have low PEF. Therefore, the photoelectric log is very useful for determining rock matrix properties.

Gamma-ray spectroscopy is the quantitative study of the energy spectra of gamma rays naturally emitted by the formation. The earth's natural radioactivity is originated from three elements: potassium (K), thorium (Th) and uranium (U), which emit gamma rays having different energy levels. A log of natural gamma ray spectroscopy is usually presented as a total gamma ray log and the weight fraction of the three radioactive elements. The weight fraction is given in percentage for potassium, while it is expressed in parts-per-million (ppm) for thorium and uranium.

Potassium is the most abundant main natural radioactivity source. It is found in illite, alkali feldspars, micas and some evaporite minerals. A log of potassium is used in determining the mineral content of a formation.

However, thorium is a trace element associated with clays and heavy minerals.

It is often a good measure of clay content. As regards uranium, it is a soluble trace element. That is why it is transported easily and can be precipitated far from its source. Uranium occurs generally in carbonates and organic materials, and its associated log is exploited in detecting organic material.

6.4 Geological Setting

The analyzed log data are recorded in four (04) Algerian exploration wells (W1, W2, W3 and W4) located in different parts in Algeria: southwestern (W1 and W2), southcenter (W3) and southeastern (W4).

Regarding the well W1, the studied depth interval (905.256-1492.7581m) corresponds to the lower Devonian reservoir whose lithological description is as follows:

- Layer L1(905-981m): SHALE gray to dark gray/black, soft to indurated, silty, micaceous, laminated, and pyritic clay, with fine layers of SANDSTONE, bright gray to beige, very fine to fine, siliceous to siliceous-clayey, locally dolomitic, fairly hard often passing into hard siltstone.
- Layer L2 (981-1133m): alternation of SANDSTONE clear gray to beige-gray and brown, very fine to fine, rarely medium, siliceous to siliceous-clayey, carbonated, pyritic, moderately hard and SHALE, dark gray to black, indurated, silty, micaceous, locally pyritic, with LIMESTONE layers, gray-beige to clear gray, cryptocrystalline, sometimes clayey, moderately hard to hard.
- Layer L3 (1133-1438m): SANDSTONE, clear gray to gray-beige and brown, fine to medium, sub-angular to rounded, siliceous to siliceous-quartzitic, pyritic, hard, locally very fine, clay-carbonated, micaceous, brittle, passing

sometimes into SILTSTONE, moderately consolidated to hard, with SHALE layers, gray to dark gray, soft to indurated, silty, micaceous, pyritic, with laminated, and fossiliferous tendency and LIMESTONE, clear gray, chalky, soft, sometimes sandy, moderately hard.

- Layer L4 (1438-1496m): SHALE, black carbonaceous, indurated, silty, micaceous, laminated, carbonated, with LIMESTONE intercalations, white and dark gray, microcrystalline, clayey, moderately hard, and intercalations of SANDSTONE, gray-beige to white, clayey, moderately consolidated (at the top). Presence of pyrite.

As regards the second well (W2), the investigated depth interval (1149.096-1386.84m) covers the lowest Devonian reservoir. Lithologically, this interval presents an alternation of LIMESTONE, white, soft, chalky, locally fossiliferous, sometimes beige, microcrystalline to crystalline, dolomitic, and SANDSTONE, clear gray to gray, very fine to fine, siliceous-clayey, moderately hard, locally micaceous, siliceous to siliceous-carbonated, very consolidated, with SHALE, dark gray to black, soft to indurated, silty, micaceous, sometimes laminated and pyritic. Presence of pyrite.

For well W3, the analyzed depth range (2579.0652-2716.2252m) corresponds to the Triassic reservoir. It is composed of the alternation of SANDSTONE, white gray to gray-beige, very fine to medium, clayey, moderately hard with fine layers of shale, gray to brown, silty, micaceous, indurated, and SHALE, clear gray to beige-gray, silty, micaceous and indurated.

Finally, the used measurement data of Well W4 are recorded between the depths of 3496.6656m and 4800.7524m. This depth interval corresponds to the Lias reservoir. It is marked by the predominance of SHALE, brown, rarely gray, silty, locally anhydritic, indurated with fine and rare layers of silt, and by the

presence of fine layers of SANDSTONE, white gray to white, soft to moderately consolidated.

6.5 Regularity Analysis Applied to Well Logs

In this section, we show the results of the regularity analysis obtained from datasets recorded in the considered four wells (Table 1). The log data corresponding, respectively, to wells W1, W2, W3 and W4 are presented in Figures 1, 2, 3 and 4. All the used logs are recorded with a sampling rate of 0.1524m.

Table 1. *Physical properties recorded in the considered wells (W1, W2, W3 and W4).*

Physical property	Symbol/ Unit	Well W1	Well W2	Well W3	Well W4
P-wave seismic velocity	Vp (m/s)	x	x		x
S-wave seismic velocity	Vs (m/s)		x		x
Bulk density	rhob (g/cm^3)	x		x	
Neutron porosity	nphi (%)	x			
Gamma Ray	GR (API)	x	x	x	x
Photoelectric absorption factor	PEF	x		x	
deep dual laterolog	LLD (Ohm.m)	x			
Array Induction Two Foot Resistivity	AT20 (Ohm.m)		x		x
Array Induction Two Foot Resistivity	AT90 (Ohm.m)		x		x
Thorium gamma ray spectroscopy	Th (ppm)	x		x	
Uranium gamma ray spectroscopy	U(ppm)	x			
Potassium gamma ray spectroscopy	K(%)			x	

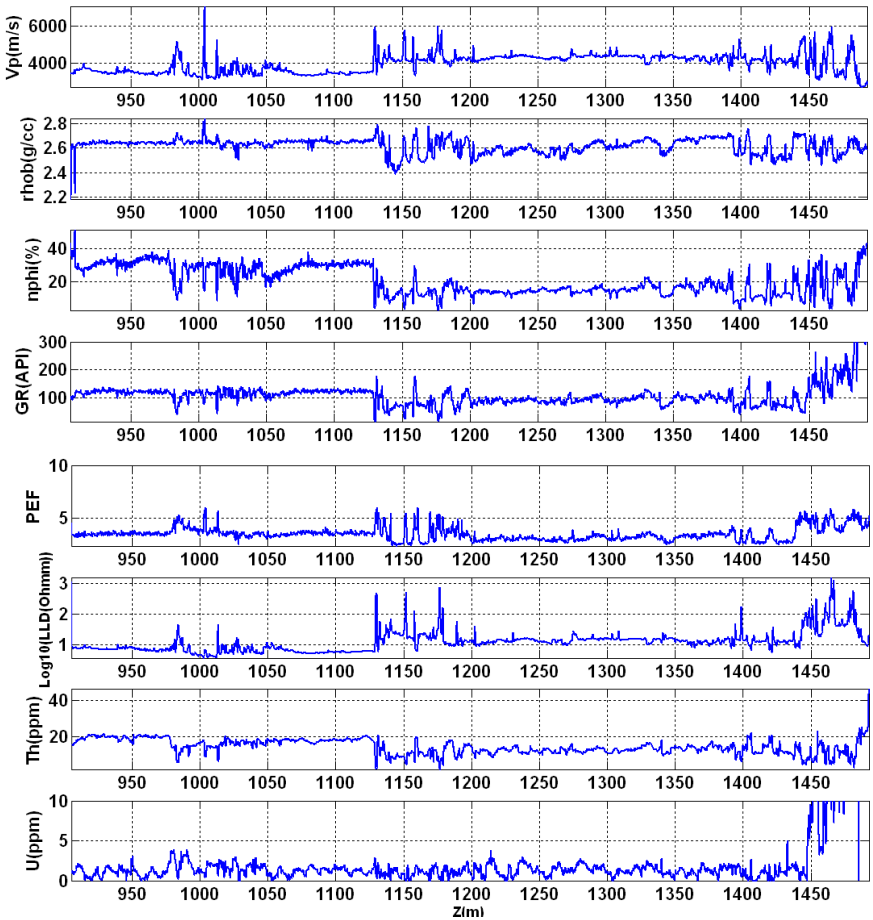

Figure 1. *Physical properties measured within the depth interval (905- 1493m) in borehole W1. Symbols as in Table 1. Log: decimal logarithm.*

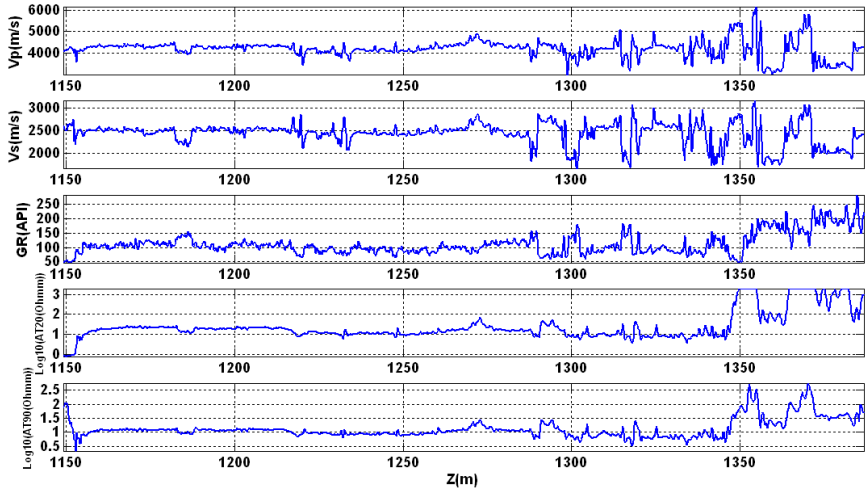

Figure 2. *Physical properties measured within the depth interval (1149 -1387m) in borehole W2. Symbols as in Table 1. Log: decimal logarithm.*

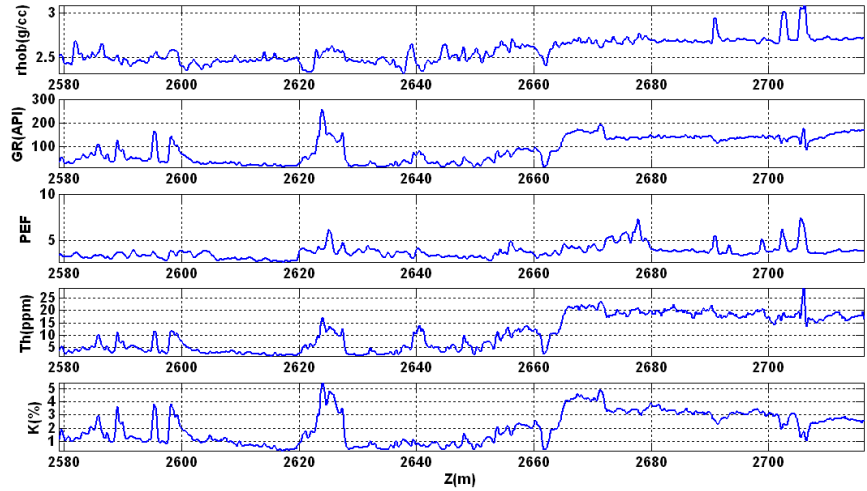

Figure 3. *Physical properties measured within the depth interval (2579-2716m) in borehole W3. Symbols as in Table 1.*

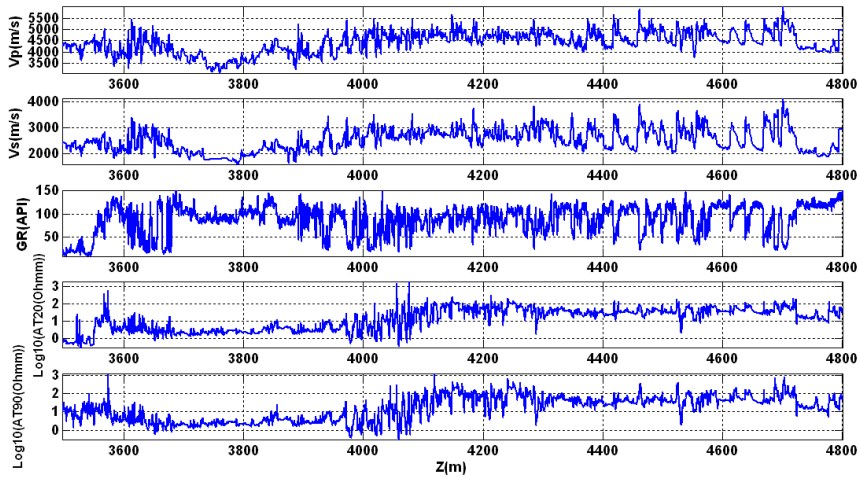

Figure 4. *Physical properties measured within the depth interval (3497-4801m) in borehole W4. Symbols as in Table 1. Log: decimal logarithm.*

As in our previous works (Gaci et al., 2010; Gaci and Zaourar, 2010, 2011a), well logs are considered as paths of mBm processes. A local regularity profile is computed for each log using the algorithm presented above. The regularity profiles obtained from the analyzed logs corresponding to wells W1, W2, W3 and W4 are illustrated, respectively, in Figures 5, 6, 7 and 8. For the needs of a lithological segmentation, the geological discontinuities crossed by the studied wells are reported on the derived regularity logs. The boundaries of the main layers are represented by red dashed lines, while limestone, sandstone and shale beds are shown, respectively, in green, yellow and black dashed lines.

The investigation of the results obtained from different datasets reveals a clear correlation of lithology with some regularity profiles, mainly those derived from Vp, Vs, rhob and nphi logs which measure the liquid-filled porosity. However, the regularity profiles derived from the other logs, specifically GR, LLD, AT20, AT90, PEF, Th, U and K logs, do not allow to recognize the different geological discontinuities on all the datasets. This may be explained by the weak

dependence of these logs on the porosity. These findings are in agreement with the results of our previous work (Gaci et al., 2010), performed on sonic logs recorded in the KTB boreholes, showing a good match between local extrema values of regularity profiles and fluid-filled fractures zones characterized by high porosity values.

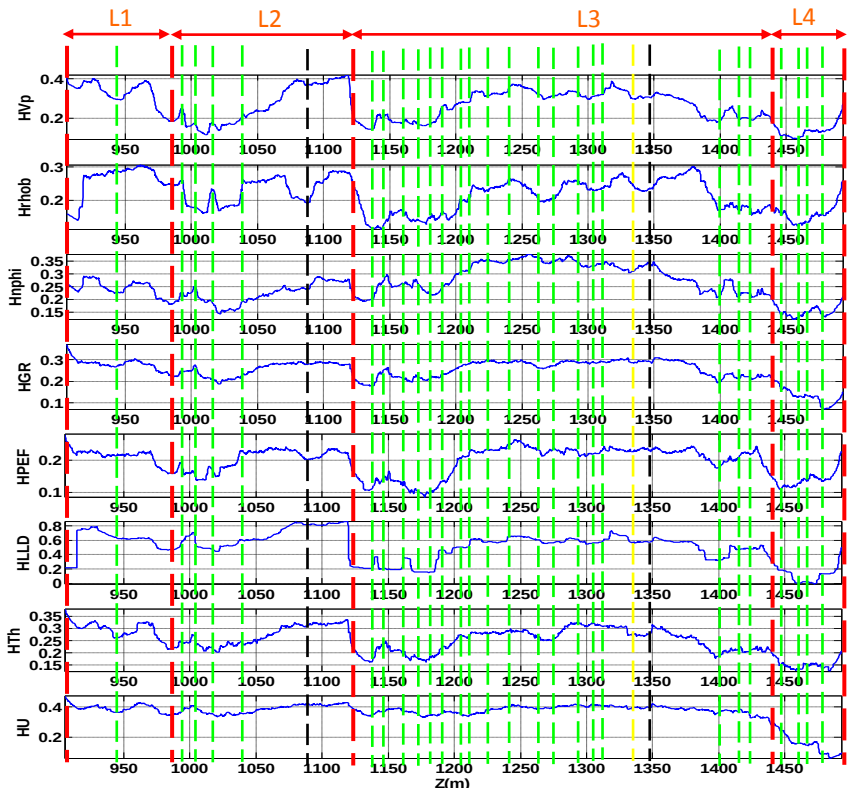

Figure 5. *Regularity profiles obtained from the physical measurements of Figure 1 (Well W1). Dashed lines: layer boundaries (in red), limestone beds (in green), sandstone beds (in yellow), and shale beds (in black).*

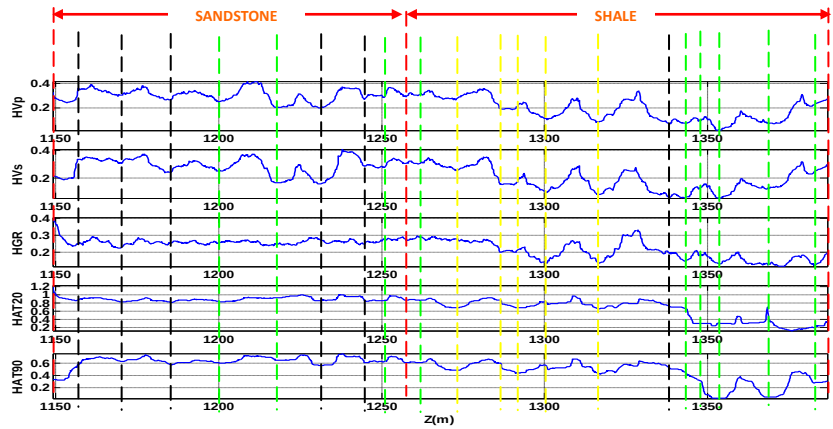

Figure 6. *Regularity profiles obtained from the physical measurements of Figure 2 (Well W2). Dashed lines: layer boundaries (in red), limestone beds (in green), sandstone beds (in yellow), and shale beds (in black).*

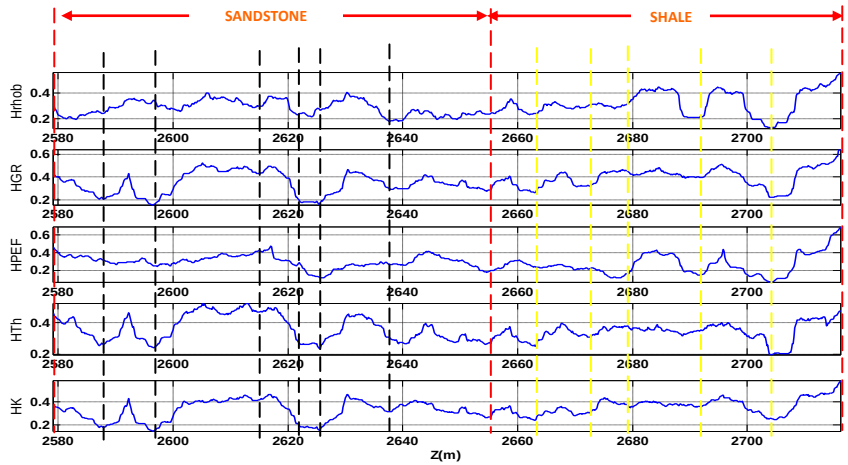

Figure 7. *Regularity profiles obtained from the physical measurements of Figure 3 (Well W3). Dashed lines: layer boundaries (in red), sandstone beds (in yellow), and shale beds (in black).*

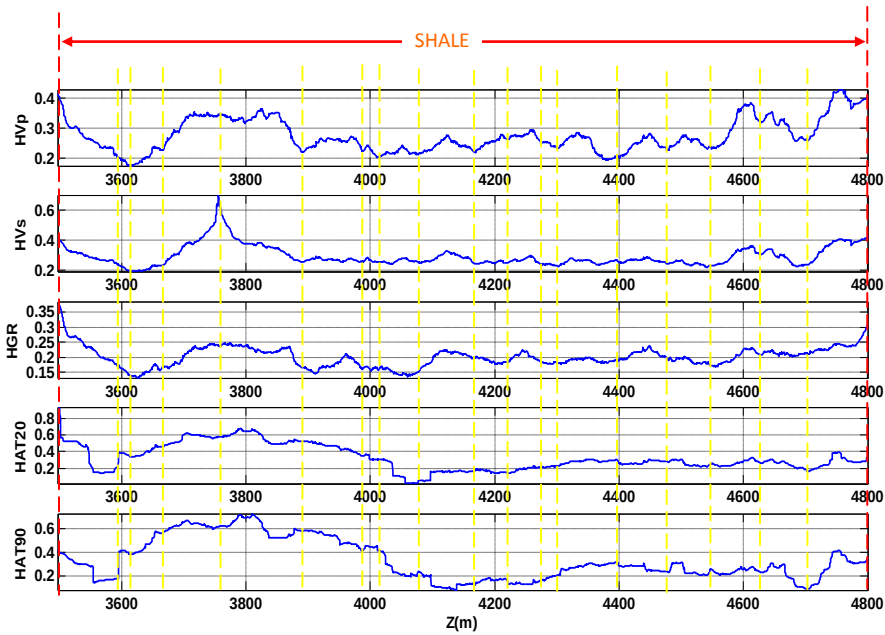

Figure 8. *Regularity profiles obtained from the physical measurements of Figure 4 (Well W4). Dashed lines: layer boundaries (in red), sandstone beds (in yellow), and shale beds (in black).*

It can be noted that on the regularity profiles derived from the ‘’porosity-dependent’’ logs, almost all the lithological discontinuities, which are either layer boundaries or thin rock beds occurred within the studied depth intervals, are marked by jumps in H value. However, some geological interfaces between layers are not noticeably identified on the regularity logs, as is the case for the interface L3-L4 (Figure 5), sandstone-shale (Figures 6-7). This statement is explained by the fact that these adjacent units present a similar lithology, thus do not exhibit a distinct lithological limit between them. In addition, an observation deserves to be noted is that some rock beds are not clearly detected on the regularity curves due to their small thicknesses. A rock bed becomes easier to identify as its thickness increases, and the smallest bed thickness that can be identified on a regularity log is about 1m.

In order to identify a relationship between a lithology and a regularity degree, H-values means are calculated for all the analyzed logs over depth intervals of the identified geological units crossed by the wells (Table 2).

Table 2. *Mean Hölder exponent values for the analyzed logs over the different depth intervals.*

Log/Well	W1				W2		W3		W4
	L1 (Sh)	L2 (Sd/ Sh)	L3 (Sd)	L4 (Sh)	(Sd)	(Sh)	(Sd)	(Sh)	(Sh)
Vp	0.34	0.26	0.27	0.14	0.31	0.19	-	-	0.27
Vs	-	-	-	-	0.29	0.18	-	-	0.29
Rhob	0.26	0.23	0.21	0.16	-	-	0.29	0.32	-
nphi	0.25	0.22	0.30	0.15	-	-	-	-	-
GR	0.28	0.25	0.26	0.13	0.26	0.20	0.34	0.40	0.20
PEF	0.22	0.20	0.20	0.14	-	-	0.30	0.26	-
LLD	0.60	0.63	0.49	0.13	-	-	-	-	-
AT20	-	-	-	-	0.90	0.62	-	-	0.32
AT90	-	-	-	-	0.63	0.44	-	-	0.34
Th	0.30	0.26	0.25	0.15	-	-	0.37	0.34	-
U	0.40	0.38	0.38	0.16	-	-	-	-	-
K	-	-	-	-	-	-	0.32	0.36	-

Sd: sandstone; Sh: shale.

For a given well, the H-values mean varies depending on the specified layer and the type of the log. Moreover, for the same log and lithology, this value is not steady as is the case of the layers L1 and L4 (well W1). Though the latter are mainly composed of shale, they correspond to different H-value means for all the investigated logs. These findings corroborate the results of our earlier researches (Gaci et al., 2010; Gaci and Zaourar, 2010, 2011a). According to the latter, the lithological layers intersected by the KTB wells, specifically amphibolite, gneiss and variegated units, exhibit very close regularity degrees, and a given lithology cannot be described by a unique H value.

Next, for each well, a correlation analysis is performed on the estimated

regularity profiles. Correlation coefficients between the regularity profiles derived from the investigated well logs are given in tables 3, 4, 5 and 6 corresponding, respectively, to wells W1, W2, W3 and W 4. The tables reveal a strong correlation between all the computed regularity profiles (except between HVp-HAT90, HGR-HAT20 and HGR-HAT90 for well W4), even if the borehole measurements are weakly correlated.

Table 3. *Correlation coefficients between the regularity profiles derived from the analyzed well logs (Well W1).*

	HVp	**Hrhob**	**Hnphi**	**HGR**	**HPEF**	**HLLD**	**HTh**	**HU**
HVp	1.000	0.681	0.728	0.839	0.801	0.788	0.917	0.635
Hrhob		1.000	0.416	0.639	0.743	0.738	0.715	0.468
Hnphi			1.000	0.762	0.618	0.505	0.668	0.613
HGR				1.000	0.751	0.760	0.911	0.874
HPEF					1.000	0.754	0.803	0.527
HLLD						1.000	0.833	0.668
HTh							1.000	0.758
HU								1.000

Table 4. *Correlation coefficients between the regularity profiles derived from the analyzed well logs (Well W2).*

	HVp	**HVs**	**HGR**	**HAT20**	**HAT90**
HVp	1.000	0.955	0.793	0.632	0.747
HVs		1.000	0.675	0.470	0.636
HGR			1.000	0.779	0.706
HAT20				1.000	0.847
HAT90					1.000

Table 5. *Correlation coefficients between the regularity profiles derived from the analyzed well logs (Well W3).*

	Hrhob	**HPEF**	**HGR**	**HTh**	**HK**
Hrhob	1.000	0.638	0.549	0.557	0.567
HPEF		1.000	0.511	0.827	0.951
HGR			1.000	0.551	0.496
HTh				1.000	0.762
HK					1.000

Table 6. *Correlation coefficients between the regularity profiles derived from the analyzed well logs (Well W4).*

	HVp	**HVs**	**HGR**	**HAT20**	**HAT90**
HVp	1.000	0.798	0.756	0.414	0.288
HVs		1.000	0.680	0.537	0.475
HGR			1.000	0.362	0.080
HAT20				1.000	0.907
HAT90					1.000

As mentioned earlier, a clear correlation is shown between the regularity profiles derived from the recorded well logs even if the latter are weakly correlated. The regularity is therefore a robust property which can be used successfully to characterize lithological heterogeneities of layers.

In the following, we aim at checking for the existence of a relation between H exponents and the recorded physical parameter (P) of the different logs recorded in the considered boreholes. The method consists of representing a scatter plot of data in "the phase plane", i.e. "Hölder exponent- physical parameter" plane (Barrière, 2007; Echelard et al., 2010). Each depth z of the log, with a physical parameter value P(z) and its estimated regularity exponent H(z) is represented by a point with coordinates (P(z), H(z)) in this plane. To enhance the analysis of the scatter diagram, the density of the points is plotted instead. By doing so, different scatter plots are represented in the "regularity-physical parameter" plane for each

log. The plots related to wells W1, W2, W3 and W4 are exposed, respectively, in Figures 9, 10, 11 and 12.

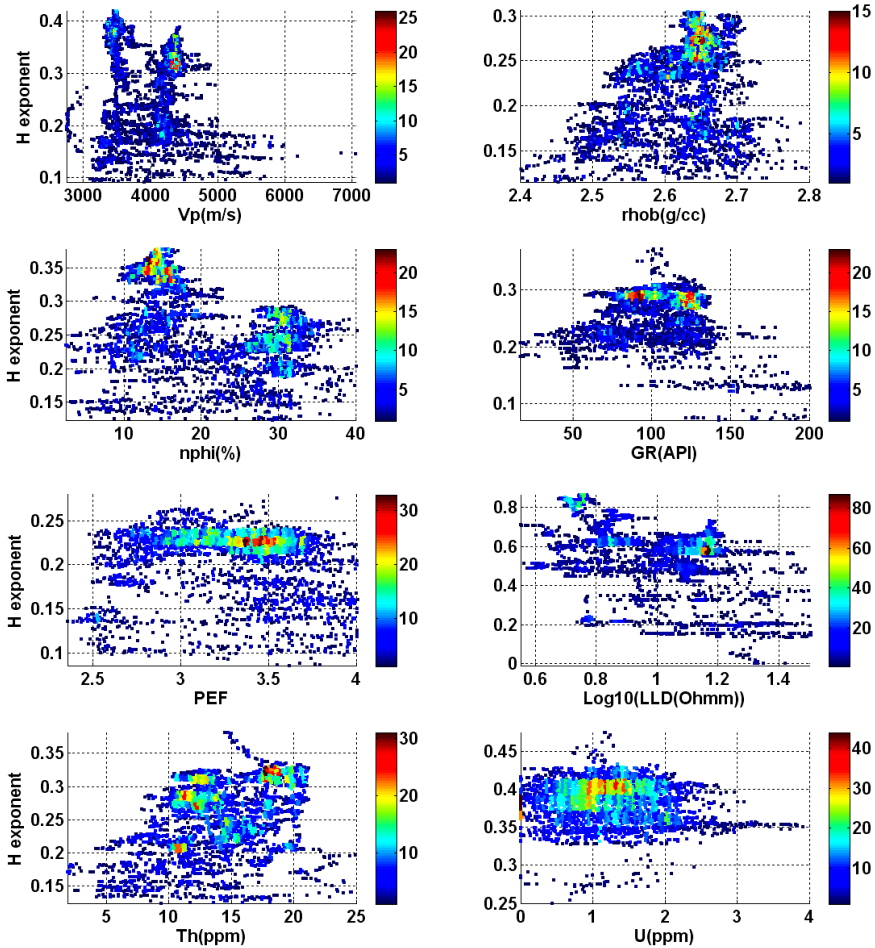

Figure 9. *Density of the scatter plots in the ''Hölder exponent- physical parameter'' plane obtained from the borehole W1 logs.*

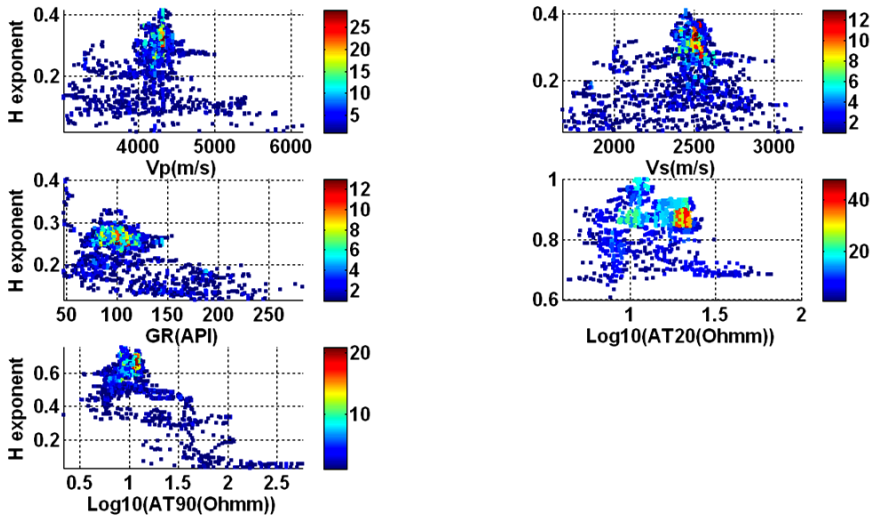

Figure 10. *Density of the scatter plots in the ''Hölder exponent- physical parameter'' plane obtained from the borehole W2 logs.*

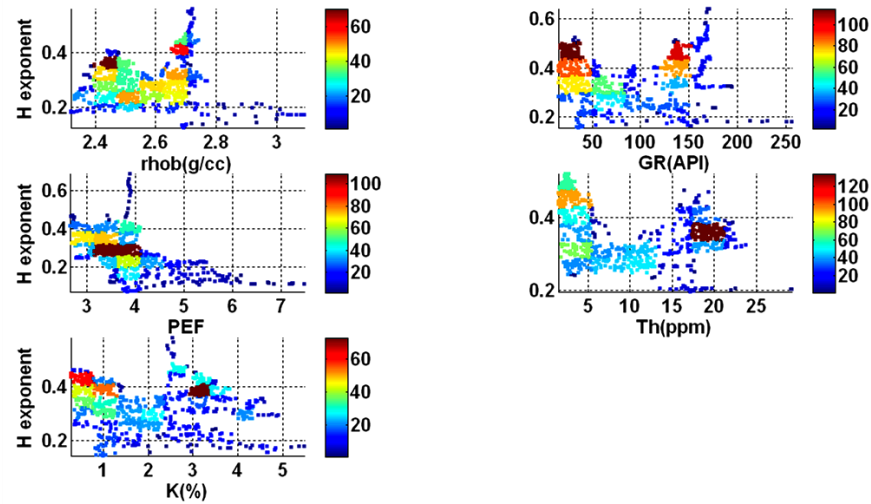

Figure 11. *Density of the scatter plots in the ''Hölder exponent- physical parameter'' plane obtained from the borehole W3 logs.*

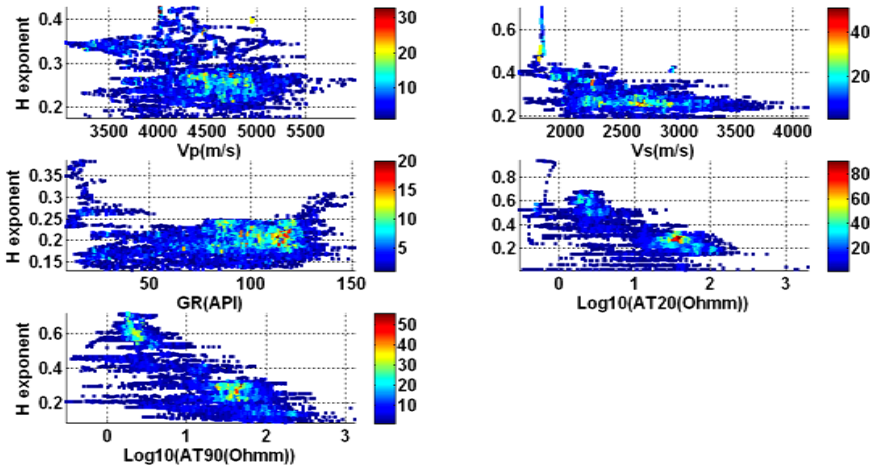

Figure 12. *Density of the scatter plots in the ''Hölder exponent- physical parameter'' plane obtained from the borehole W4 logs.*

All these diagrams reveal an irregular distribution of the points, and on each diagram very scattered regularity exponents correspond to the same value of the considered physical parameter. The scatter plots do not then allow to infer a clear function between P(z) and H(z), and the investigated logs cannot be described by self-regulated multifractional processes (SRMPs).

Considering the aforementioned results, a correlation analysis is carried out on P(z) and H(z) logs so as to determine the relation between the physical parameter and its estimated regularity (Table 7). The correlation coefficients obtained from the analyzed datasets show a weak correlation between logs and their computed regularity, except for U log (well W1), AT20 and AT90 logs (well W2), GR log (wells W2-W3), Vs log (well W4). To notice also that for some logs (Vp, Vs, GR, PEF, and Th), the correlation coefficients take positive and negative values. These observations should be checked on a large number of datasets in order to confirm the weak correlation for all the types of logs.

Table 7. *Correlation coefficients between the logs and their estimated regularity profiles for all the datasets.*

Well/ Log	Vp	Vs	rhob	nphi	GR	PEF	LLD	AT20	AT90	Th	U	K
W1	-0.13	-	0.33	-0.31	-0.42	-0.46	-0.33	-	-	0.38	-0.80	-
W2	0.08	0.21	-	-	-0.57	-	-	-0.68	-0.60	-	-	-
W3	-	-	0.10	-	-0.53	0.05	-	-	-	-0.27	-	-0.11
W4	-0.32	-0.55	-	-	0.04	-	-	-0.40	-0.48	-	-	

6.6 Conclusion

This paper presents the results of a regularity analysis carried out on different well logs recorded in four Algerian exploration boreholes drilled in different geological contexts. The investigated datasets contain very diversified logs, and are considered here as paths of multifractional Brownian motion (mBm).

The regularity profiles independently derived from the logs, particularly those obtained from the "porosity-dependent" logs (sonic, density and neutron), are significantly correlated with the lithology; the lithological discontinuities correspond to abrupt changes in the Hölder exponent value. Moreover, for a given well, the derived regularity curves are strongly correlated.

The obtained results show that no relationship can be drawn between the measured physical parameter and its estimated regularity exponent. Therefore, the logs cannot be considered as realizations of a self-regulated multifractional process (SRMP). Besides, low correlation coefficients are generally observed between the physical measurements and the Hölder exponents for the available logs. In our upcoming researches, we will be trying to accurately quantify the regularity exponent and the relationship between the log and its estimated regularity profile. In addition, the regularity analysis will be extended to a very large dataset composed of very diversified well logs.

Acknowledgment

I acknowledge SONATRACH- Division Exploration for providing the data published in this paper.

References

[1] Ayache, A. and Taqqu, M.S., 2005. Multifractional process with random exponent. Publ. Mat., 49, 459-486.

[2] Barrière, O., 2007. Synthèse et estimation de mouvements browniens multifractionnaires et autres processus à régularité prescrite. Définition du processus auto-régulé multifractionnaire et applications (in french). PhD thesis. Univ. of Nantes (France).

[3] Benassi, A., Jaffard, S. and Roux, D., 1997a. Elliptic Gaussian random processes. Revista Matemática Iberoamericana, 13 (1), 19-90.

[4] Benassi, A, Jaffard S, Roux D, 1997b. Gaussian processes and pseudodifferential elliptic operators. Rev. Mat. Iberoamericana. 13 (1), 19-81.

[5] Bicego, M. and Trudda, A., 2010. 2D shape classification using multifractional brownian motion. Lecture Notes in Computer Science, 5342, 906-916.

[6] Cersosimo, D. O. and Wanliss, J.A., 2007. Initial studies of high latitude magnetic field data during different magnetospheric conditions. Earth Planets Space, 59 (1), 39-43.

[7] Echelard, A., Barriere, O. and Lévy-Véhel, J., 2010. Terrain modelling with multifractional Brownian motion and self-regulating processes, ICCVG 2010, 6374, 342-351. Available at:
http://hal.archives-ouvertes.fr/docs/00/53/89/07/PDF/mbf_self-regulating.pdf.

[8] Gaci, S., Zaourar, N., Hamoudi, M. and Holschneider, M., 2010, Local regularity analysis of strata heterogeneities from sonic logs. Nonlin. Processes Geophys., 17, 455-466. Available from :
www.nonlin-processes-geophys.net/17/455/2010/doi:10.5194/npg-17-455-2010.

[9] Gaci, S. and Zaourar, N., 2010. A new approach for the investigation of the local regularity of borehole wire-line logs. J. hydrocarb. mines environ. res., 1(1), 6-13.

[10] Gaci, S. and Zaourar, N., 2011a. Heterogeneities characterization from velocity logs using multifractional Brownian motion. Arab. J. Geosci. 4:535-541, doi: 10.1007/s12517-010-0167-5.

[11] Gaci, S. and Zaourar, N., 2011b. Two-Dimensional Multifractional Brownian Motion- Based Investigation of Heterogeneities from a Core Image, Advances in Data, Methods, Models and Their Applications in Geoscience, Dongmei Chen (Ed.), ISBN: 978-953-307-737-6, InTech. Available from: http://www.intechopen.com/articles/show/title/two-dimensional-multifractional-brownian-motion-based-investigation-of-heterogeneities-from-a-core-i.

[12] Gaci, S., Zaourar, N., Briqueu, L., and Hamoudi, M., 2011. Regularity Analysis of Airborne Natural Gamma Ray Data Measured in the Hoggar Area (Algeria), Advances in Data, Methods, Models and Their Applications in Geoscience, Dongmei Chen (Ed.), ISBN: 978-953-307-737-6, InTech. Available from: http://www.intechopen.com/articles/show/title/regularity-analysis-of-airborne-natural-gamma-ray-data-measured-in-the-hoggar-area-algeria.

[13] Hardy, H. H. and Beier, R. A., 1994. Fractals in Reservoir Engineering, World Scientific, Singapore, 359 pp.

[14] Hewett, T. A., 1986. Fractal Distributions of Reservoir Heterogeneity and Their Influence on Fluid Transport, in: SPE Ann. Tech. Conf., New Orleans, Society of Petroleum Engineers (SPE) Paper 15386.

[15] Keylock, C. J., 2010. Characterizing the structure of nonlinear systems using gradual wavelet reconstruction, Nonlinear Processes in Geophysics, 17(6), 615-632.

[16] Kolmogorov, A. N., 1940. Wienersche Spiralen und einige andere interessante Kurven in Hilbertchen Raume, Doklady, 26, 115-118.

[17] Li, M., Lim, S.C., Hu, B-J. and Feng, H., 2007. Towards describing multi-fractality of traffic using local Hurst function. Lecture Notes in Computer Science, 4488, 1012-1020.

[18] Luo, P.-P., Wang, L-F., Fan, B., Zhang, F., 2012. Numerical simulation of infiltration laws of grouts in random aperture based on multi-fractional Brownian motion, Chinese J. Geot. Eng., 34(2), 309-316.

[19] Mandelbrot, B. B. and Van Ness, J., 1968. Fractional Brownian motion, fractional noises and applications, SIAM Rev., 10, 422-437.

[20] Mandelbrot, B. B., 1975. Les Objets Fractals: Forme, Hasard et Dimension. Flammarion, Paris.

[21] Mandelbrot, B. B., 1977. Fractals: Form, Chance, and Dimension. W.H. Freeman and Co., San Francisco.

[22] Peltier, R. F. and Lévy-Véhel, J., 1994. A New Method for Estimating the Parameter of Fractional Brownian motion, INRIA RR 2396.

[23] Peltier, R. F. and Lévy-Véhel, J., 1995. Multifractional Brownian Motion: Definition and Preliminaries Results, INRIA RR 2645.

[24] Wanliss, J. A., 2005. Fractal properties of SYM-H during quiet and active times. Journal of Geophysical Research, Vol. 110, No. A03202, pp 12. doi:10.1029/2004JA010544.

[25] Wanliss, J. A. and Cersosimo, D.O., 2006. Scaling properties of high latitude magnetic field data during different magnetospheric conditions. Proceedings 8th International Conference Substorms, Banff, Canada, 325-329.

[26] Wei, H. L., Billings, S. A., Balikhin, M., 2004. Analysis of the geomagnetic activity of the Dst index and self-affine fractals using wavelet transforms, Nonlinear Processes in Geophysics, 11(3), 303-312.